JTTEE5 11:387-392

Effect of Substrate Surface Roughness on the Adherence of NiCrAlY Thermal Spray Coatings

Ines Hofinger, Karen Raab, Jörg Möller, and Manfred Bobeth

(Submitted 3 January 2001; in revised form 27 July 2001)

The adherence of plasma sprayed NiCrAlY bond coats can be improved by an appropriate substrate surface finish. The interface fracture energy for crack propagation along the coating/substrate interface has been measured for different surface roughness by means of a specially designed four-point bending test. An increase of the interface fracture energy of about 15% was observed for a three times higher surface roughness. In addition, four-point bending tests with the coating on the side face of bending specimens were performed to analyze the fracture and spalling behavior of the coatings both under large tensile and compressive substrate deformations.

Keywords crack propagation, interface fracture energy, NiCrAlY bond coat, surface roughness, thermal spray coating

1. Introduction

Thermal spraying is commonly used to manufacture wear-, corrosion-, and heat-resistant coatings for various technical applications, in particular to enable an increase of the energetic efficiency by running at higher temperature. The lifetime of the coatings under service conditions can be limited by their fracture and loss of adherence under mechanical loads. Depending on the loading conditions, cracks perpendicular and parallel to the coating develop, especially along the coating/substrate interface. Such damage has been investigated in detail for thermal barrier coatings,[1,2] where appropriate techniques for measuring the coating/substrate interface fracture energy have been developed.[3,4] To avoid delamination of the coating, it is now standard industrial practice to grit blast the substrate before depositing thermal spray coatings. An appropriate roughness of the substrate surface is suited to suppress delamination by increasing the effective interface fracture energy.

The aim of the present paper is two-fold. First, the general fracture and spalling behavior of the coating under high load due to large substrate deformations is characterized by means of bending experiments with the coating on the side-face of bending specimens. In this way, both graded tensile and compressive loads were realized at once.[5] Second, we present a new, specially designed four-point bending test, which allowed measurement of the interface fracture energy for different substrate roughnesses.

Ines Hofinger, Jörg Möller, and **Manfred Bobeth,** Dresden University of Technology, Institute of Materials Science, Hallwachsstrasse 3, 01069 Dresden, Germany; and **Karen Raab,** Caterpillar Inc., P.O. Box 1875, Peoria, IL 61656-1875. Contact e-mail: Raab_Karen_R@cat.com.

2. Thermal Spray Processing and Surface Characterization

For the present investigations, NiCrAlY powder (Sulzer Metco 461, Sulzer Metco, Westbury, NY) was plasma sprayed onto 76.39 × 9.48 × 3.12 mm^3 steel beams. Both the NiCrAlY bond coat and the mild steel SAE 1010 are characterized by a Young's modulus of 210 GPa and a Poisson's ratio of 0.3. The tensile strength of the NiCrAlY bond coat was previously determined as 375 MPa.[6] The tensile strength of the steel substrate was 325 MPa, the yield strength was 180 MPa, and the hardness was determined as 95 HB.[6]

The coatings were deposited by means of the model 9MB plasma spray equipment (Sulzer Metco) using standard recommended parameters. To this end, the beams were attached to the outside of two drums of 200 mm diameter. Before coating deposition, the beams were grit blasted by hand with aluminum oxide grit. On each drum, one part of each beam was grit blasted while the other part was protected with a metal shield. This was done to obtain two different surface roughnesses at fixed

Nomenclature

G_{ss}	steady-state energy release rate
G_c	interface fracture energy
M_b	bending moment per sample width
F	applied force
l	spacing between the inner and outer loading lines
b	sample width
h_1	thickness of thermal spray coating
h_2	thickness of substrate
h_d	thickness of stiffening layer
E_1	Young's modulus of thermal spray coating
E_2	Young's modulus of substrate
E_d	Young's modulus of stiffening layer
ν_1	Poisson's ratio of thermal spray coating
ν_2	Poisson's ratio of substrate
ν_d	Poisson's ratio of stiffening layer

Table 1 Grit Blasting Parameters

Drum Number	Sample Number	Grit Size, mm	Stand-Off Distance, mm	Blast Pressure, MPa (psi)
1	A	0.15	75	0.30 (40)
1	C	1.00	75	0.69 (100)
2	B	0.15	75	0.69 (100)
2	D	1.00	75	0.69 (100)

spraying conditions (Table 1). The drum was spun at 360 rpm while the robot holding the plasma spray equipment traversed at 7 mm/s.[7]

Two different thicknesses of the thermal spray coatings combined with three substrate surface roughnesses were produced. The parameters of the investigated samples are listed in Table 2. The surface roughnesses resulting from grit blasting were analyzed using a surface profilometer (Somicronic Surfascan, St. Andre de Carcy, France) with the stylus ST084 (10 μm tip radius, 90° tip angle) The measured length was 4.8 mm using 0.8 mm cut-off lengths to obtain the surface finish parameters. The surface profiles of the samples are shown in Fig. 1.

3. Fracture Behavior of Coatings

To elucidate the fracture and spalling behavior of thermal spray coatings, four-point bending experiments were carried using specimens with the coating on the side-face of the bending bar (Fig. 2). The bending deformation of the substrate induces a graded load in the coating ranging from compression to tension. In this way, crack initiation and propagation within the coating can be observed at once under compressive and tensile load.[5] Prior to bending experiments, the top and bottom sides of the coated samples (cf. Fig. 4) were ground with SiC-paper, grit 220.

3.1 Coating Failure Under Tension

Under tensile load, thermal spray coatings typically fail by forming straight through-thickness cracks, running perpendicular to the coating from the specimen edge toward the neutral axis. Cracks with sufficiently large crack opening can easily be detected by light microscopy (Fig. 3). The enlarged view in Fig. 3 shows a considerable roughness of the crack faces, which is presumably caused by the special microstructure of the thermal spray coatings exhibiting a series of imperfections (porosity or oxide films between splats). Side views of the fractured coating (Fig. 4,5) revealed a pattern of parallel cracks. The rugged crack faces visible in the enlarged views in Fig. 6 obtained by laser scanning microscopy (LSM) reflect again the heterogeneous microstructure of the coating. The cracks probably propagate along the interfaces between the splats (see also Ref. 8).

After through-thickness cracking, the crack opening width strongly increases with further bending, reaching values up to 0.2 mm (Fig. 5). This large crack opening presumably is due to the propagation of delamination cracks along, or very near, the coating/substrate interface, starting at the through-thickness cracks. Despite the large substrate deformation of greater than 3%, only partial delamination was observed, but no spallation. A quantitative analysis of light microscopic images of the effect of substrate roughness on delamination on the base as shown in Fig. 5 was impractical. In this respect, the modified bending test described in Section 4 is more quantitative.

Table 2 Substrate Roughness and Coating Thickness Data of Samples

	Substrate Surface Roughness, μm	Thickness of Thermal Spray Coating, mm
Samples A	$R_a = 1.3$ $R_z = 9.6$	0.25
Samples B	$R_a = 2.2$ $R_z = 15.4$	0.50
Samples C	$R_a = 4.8$ $R_z = 29.7$	0.25
Samples D	$R_a = 4.8$ $R_z = 29.7$	0.50

The observed spacing between the parallel cracks was approximately four to six times the coating thickness. These values fit well with a shear lag model for determining the crack spacings in the case of thin films on ductile substrates (cf. for example Ref. 9). According to this model, typical crack spacings l_c should obey the condition We $\sqrt{3} < (\sigma_Y^S l_c)/(\sigma_c^C d_c) < 2\sqrt{3}$, where d_c is the coating thickness, σ_Y^S is the yield strength of the substrate, and σ_c^C a is the tensile strength of the coating. Using the values for σ_Y^S and σ_c^C given above, one obtains the relations $3.6 < l_c/d_c < 7.2$, which is in good agreement with the observations.

3.2. Coating Failure Under Compression

Under compressive load, the coatings showed no large-scale damage at all. A view of the coating cross section on a smaller scale (Fig. 7) revealed crack patterns, which suggest the formation of cracks oriented in the coating that are referred to as shear cracks. The compressive stress in the coating obviously is relieved by the formation of numerous microcracks. Note that some regions have rotated as indicated by the different directions of grinding scratches. The present findings suggest that the special microstructure of thermal spray coatings is suited to suppress catastrophic macrocracks by means of microcracking. In this way, large-scale delamination and spalling of the coating are avoided. The absence of macroscopic delaminations shows that the toughness of the coating/substrate interface is comparatively high. A quantitative analysis of the interface fracture energy is given in the next section.

4. Modified Bending Test for Determining the Interface Fracture Energy G_c

A special four-point bending test proposed by Charalambides[10] allows determination of the interface fracture energy, G_c, between coating and substrate for different material properties. The application of this method is, however, restricted to cases for which the fracture toughness of the coating is sufficiently high to prevent fracture of the coating. Otherwise, vertical cracks would be formed which decrease the elastic energy in the coating. Another precondition is a sufficiently large coating thickness to provide a sufficient amount of elastic energy, which

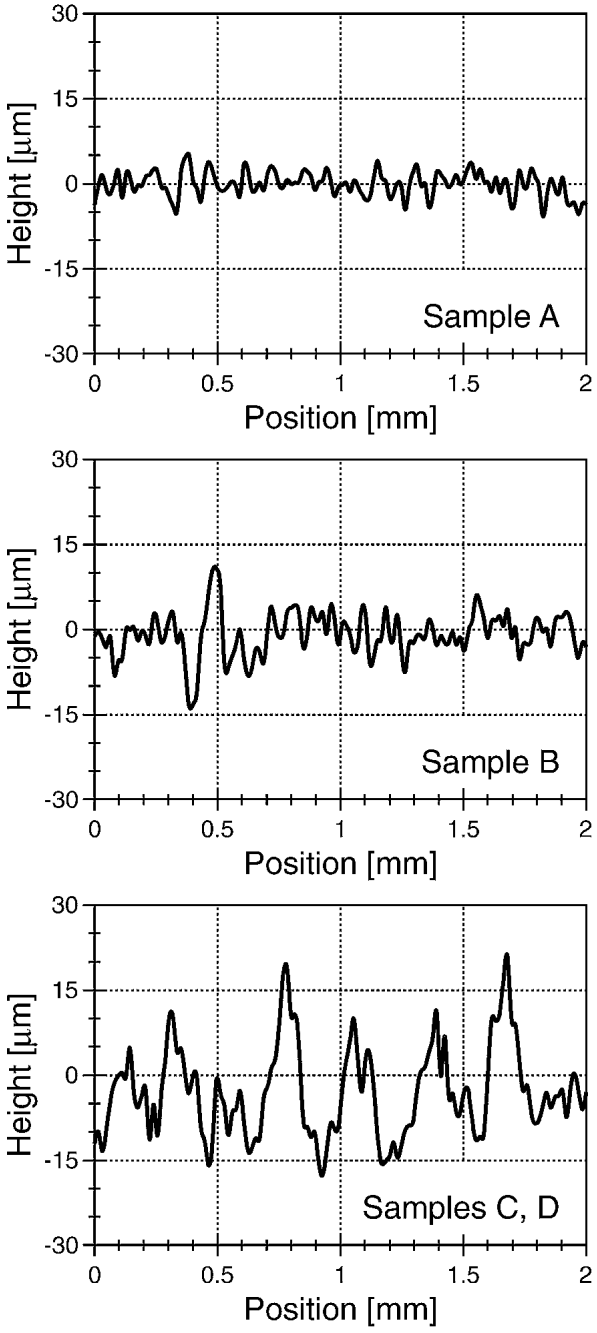

Fig. 1 Surface roughness measurements of steel specimens subject to different grit blasting procedures

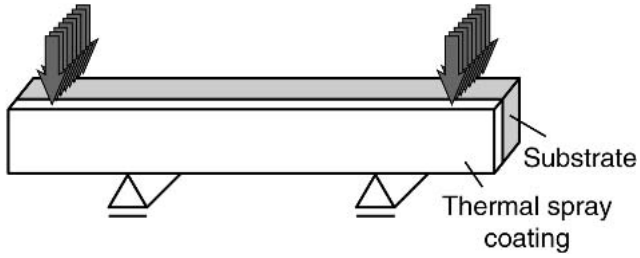

Fig. 2 Four-point bending specimen with thermal spray coating

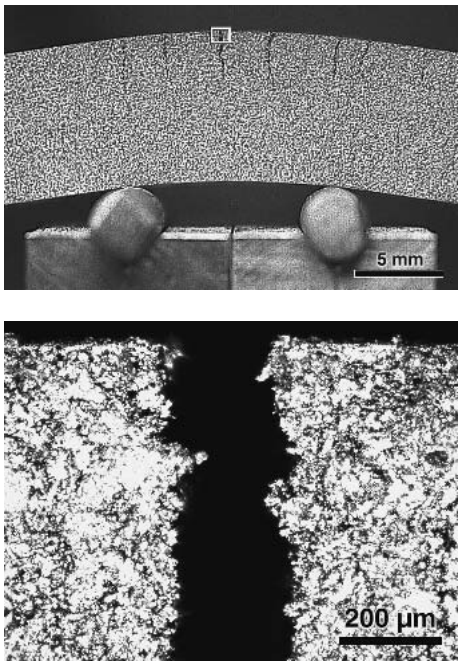

Fig. 3 View of the coated side of sample B in the final bending state (maximum deformation) with an enlarged image of one crack in the tensile region

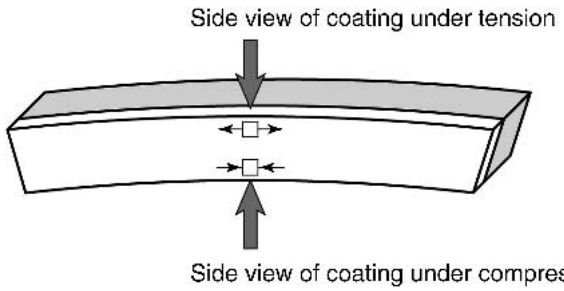

Fig. 4 Illustration of the views of the images in Fig. 5-7

is necessary for crack propagation along the interface.[11] A modification of the test by Charalambides, presented in Ref. 3, enables the measurement of the interface fracture energy also for thin coatings. The modification consists of a reinforcement of the coating by a stiffening layer bonded onto the top of the coating (Fig. 8). This stiffening layer affects an increased driving force required for crack propagation.

The modified Charalambides test has been proved on plasma sprayed ZrO_2-ceramic coatings.[3] Under displacement controlled testing, stable crack propagation during increasing load took place. In this general case of increasing load, the evaluation of G_c requires numerical evaluation, e.g., by the finite element method.

For crack propagation under constant load, corresponding to steady-state crack propagation (i.e., the crack length is large compared with the thicknesses of the coating and the stiffening layer), an analytic solution for the energy release rate exists. In

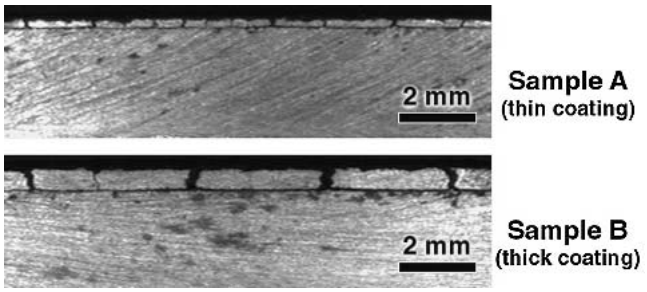

Fig. 5 Images of samples A and B after four-point bending showing through-thickness cracks in the coating as well as delamination cracks between coating and substrate (for a side view of coating under tension, see Fig. 4)

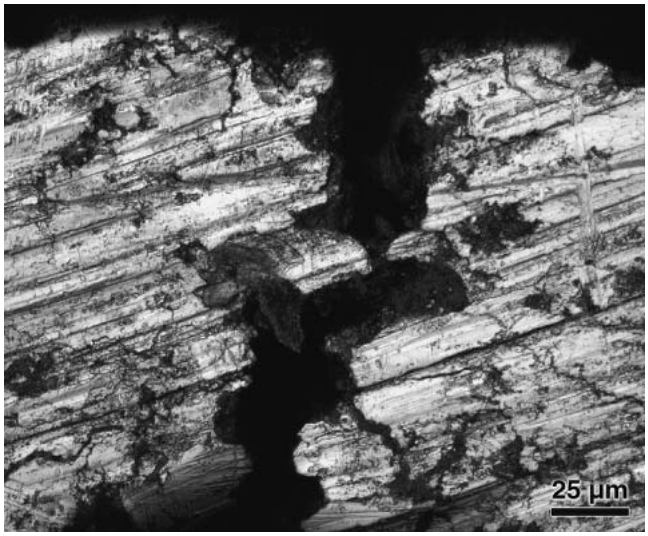

Fig. 6 LSM image of rough crack faces of through-thickness crack formed under tensile load (sample A); scratches are due to grinding during sample preparation

this special case, the interface crack has to propagate between the inner loading lines. To obtain long cracks, it is preferable to place the notch asymmetrically, close to one of the inner loading lines (Fig. 8). During four-point bending, an interface crack propagates toward the other inner loading line.

For steady-state crack propagation, the energy release rate, G_{ss}, equals the interface fracture energy, G_c. Under assumption of Hook's law, it is obtained from the composite beam theory as[3]

$$G_{ss} = \frac{M_b^2 (1 - \nu_2^2)}{2E_2} \left(\frac{1}{I_2} - \frac{1}{I_c} \right) \quad \text{(Eq 1)}$$

with the bending moment per sample width b

$$M_b = \frac{Fl}{2b} \quad \text{(Eq 2)}$$

and the second moments of inertia per sample width

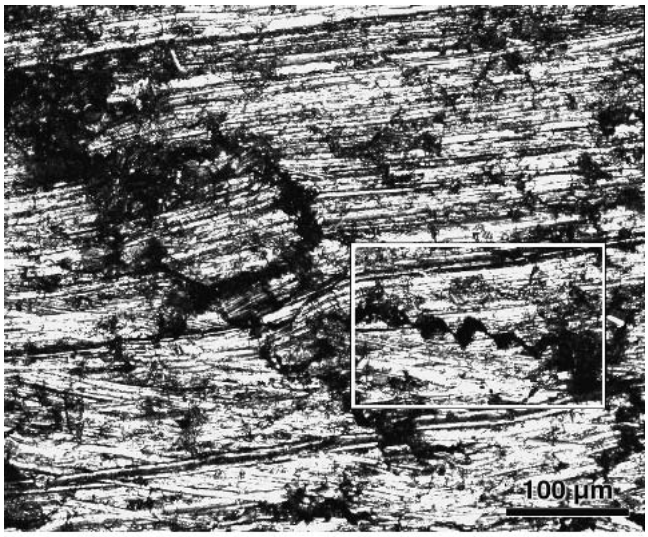

(a)

(b)

Fig. 7 LSM images of coating failure under compressive load (sample B); the detail shows the rough crack faces of a shear crack (for a side view of the coating under compression, see Fig. 4)

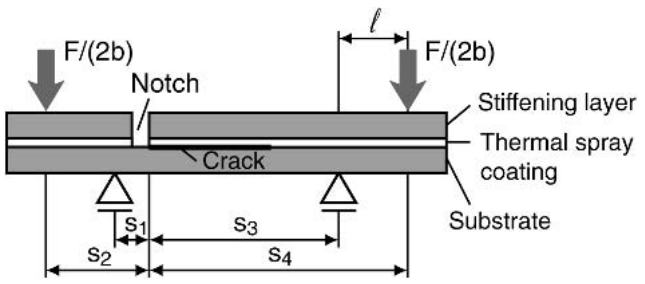

Fig. 8 Modified four-point bending specimen with asymmetrical interface crack

$$I_2 = \frac{h_2^3}{12} \quad \text{(Eq 3)}$$

and

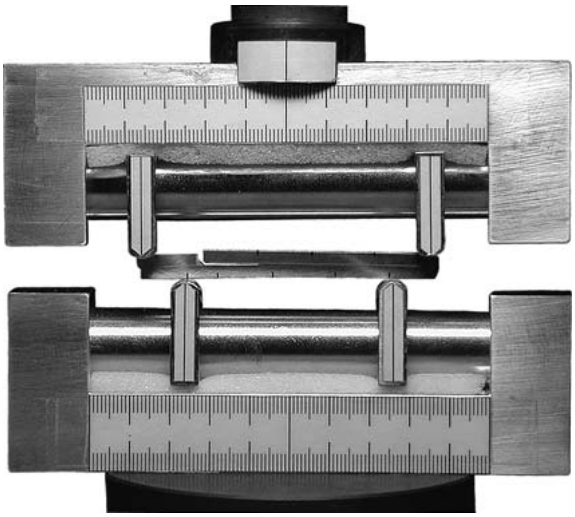

Fig. 9 Experimental setup with specimen for determination of the interface fracture energy

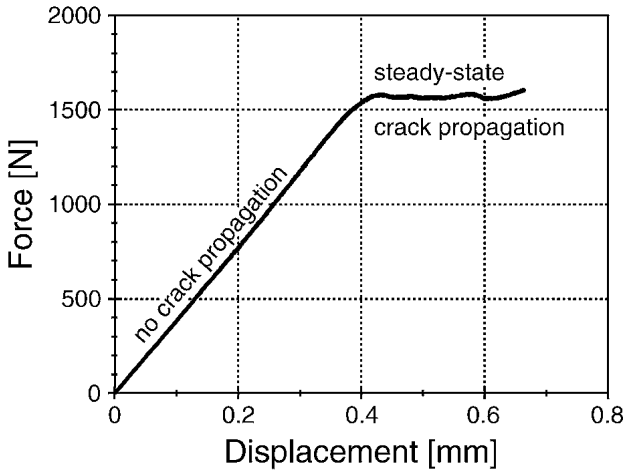

Fig. 10 Force-displacement plot for determination of the interface fracture energy

Table 3 Positions of the Inner and Outer Loading Lines During the Three Loading Steps (a)

Step	s_1, mm	s_2, mm	s_3, mm	s_4, mm
1	4	14	18	28
2	4	14	34	44
3	4	14	48	58

(a) For definitions of s_1-s_4, see Fig. 8.

$$I_c = \frac{h_2^3}{3} + \kappa\frac{h_1^3}{3} + \mu\left(\frac{h_d^3}{3} + h_d^2 h_1 + h_1^2 h_d\right) - \frac{[h_2^2 - \kappa h_1^2 - \mu(h_d^2 + 2h_1 h_d)]^2}{4(h_2 + \kappa h_1 + \mu h_d)} \quad \text{(Eq 4)}$$

where

$$\kappa = \frac{E_1(1-\nu_2^2)}{E_2(1-\nu_1^2)} \quad \text{and} \quad \mu = \frac{E_d(1-\nu_2^2)}{E_2(1-\nu_d^2)} \quad \text{(Eq 5)}$$

where F denotes the applied force and l is the spacing between the inner and outer loading lines (see Fig. 8). The parameters E, ν, and h represent the Young's modulus, Poisson's ratio, and layer thickness, respectively. The subscripts d, 1, and 2 refer to the stiffening layer, the thermal spray coating, and the substrate, respectively.

For the present experiments, the stiffening material was identical to the substrate material ($E_d = E_1 = E_2$, $\nu_d = \nu_1 = \nu_2$). For this special case, $\kappa = 1$ and $\mu = 1$ and Eq. (4) takes the simple form

$$I_c = \frac{h_2^3}{3} + \frac{(h_1 + h_d)^3}{3} - \frac{[h_2^2 - (h_1 - (h_1 + h_d)^2]^2}{4(h_2 + h_1 + h_d)} \quad \text{(Eq 6)}$$

The stiffening layer was bonded to the thermal spray coating with the structural adhesive Scotch-Weld 2214 (3M Corp., St. Paul, MN) . To cure the adhesive, the samples were heated to 90 °C for 2 h and afterward to 160 °C again for 2 h. To improve the adherence between the adhesive and the stiffening layer, the roughness of the layer surface was increased by sandblasting.

The bending experiments were carried out with the model 8511plus servo-hydraulic mechanical testing machine (Instron, Canton, MA). To create a short precrack, four-point bending with a small spacing between the inner loading lines was applied ($s_3 = s_1$ and $s_4 = s_2$, Fig. 8).

The precracked specimens were loaded three times with different loading lines as listed in Table 3. At every step, the delamination crack has propagated stably and stopped by approaching the right inner loading line because of a reduction of the driving force G. Before continuing with the next step, the positions of the right loading lines were shifted to the right.

The experimental setup and a characteristic force-displacement plot measured during loading are shown in Fig. 9 and 10, respectively. Figure 10 shows an initial load increase until a critical value F_c of the force is reached and crack propagation starts. In this plot, a region of constant load corresponding to steady-state crack propagation can be seen. The application of three loading steps allows three measurements of the interface fracture energy G_c to be carried out for one specimen.

The interface fracture energy G_c was measured for samples A, B, and D. Inspection of the crack faces gave no indication that the "interface crack" considerably deflected into the coating. The appearance of the crack face on the substrate side was similar to the substrate surface before thermal spray coating. However, it cannot be excluded strictly that the crack propagated also very close to the interface within the coating. The values of the obtained interface fracture energy G_c of the investigated samples are plotted in Fig. 11 as a function of the surface roughness. An increase of the substrate surface roughness by a factor of three affects an increase of the interface fracture energy of about 15%. The error bars in Fig. 11 represent the corresponding measurement errors. Although the error bars are of the same order of magnitude as the increase in the interface energy, the mean values show a uniform increase.

The comparatively high value of the interface fracture energy of ≥500 N/m presumably is due to the plastic deformation near

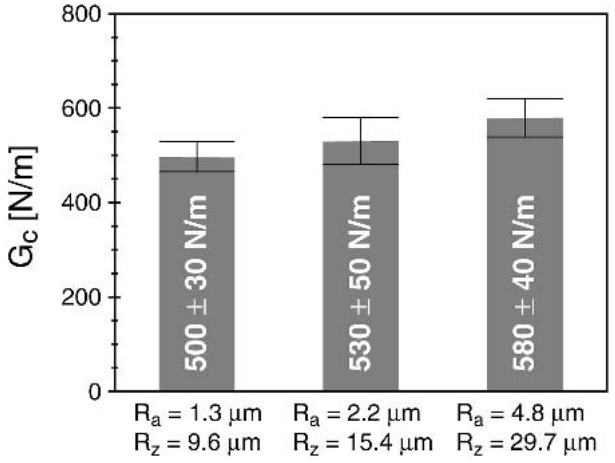

Fig. 11 Measured interface fracture energy G_c versus substrate surface roughness

the advancing crack tip. The reason for the increase of the fracture energy with increasing surface roughness is not clear. In comparison with a planar interface, a rough interface leads to an increased interface area and consequently, to an increased interface fracture energy referred to the projected area. When two rough interfaces are compared, an increase in the real interface area results if the ratio of the amplitude and wavelength of roughness increases.

Another reason for the increased fracture energy of rougher interfaces could be connected with the so-called mode mixity effect (cf. for example, Ref. 12 and references therein). As a typical trend, the interface fracture energy has been found to increase with the phase angle of loading, which characterizes the relative shear to opening, experienced by the crack faces near the tip. This phase angle influence has been related in Ref. 13 to the interface roughness and plasticity of the material. To elucidate the relevant mechanisms of the roughness effect for the present metal-metal interface, extended theoretical modeling of crack propagation is certainly needed.

5. Conclusions

NiCrAlY bond coats deposited by thermal spraying onto steel showed a very good adherence. No spallations occurred either under tensile or compressive loads induced by substrate deformations exceeding 3%. Large tensile stresses in the coating cause the formation of a pattern of parallel through-thickness cracks, whereas compressive stresses are relieved obviously by microcracking and shear crack formation within the coating.

The measured interface fracture energies from 500-580 N/m indicate that crack propagation along the NiCrAlY/steel interface is accompanied by a large amount of plastic deformation in the coating and/or substrate. The fracture energies are about one order of magnitude higher than those measured for crack propagation along a ZrO_2/steel interface.[3,4] The measurements revealed a significant influence of the substrate roughness on the interface fracture energy. In the considered roughness range, an increase of the fracture energy of 15% was achieved by increasing the roughness from R_a = 1.3-4.8 μm. A theoretical analysis of this effect was given in Ref. 12.

Acknowledgments

The authors would like to thank Wolfgang Pompe from Dresden University of Technology Dresden, Institute of Materials Science, for valuable discussions. In addition, the authors would like to express their sincere gratitude to Karan Shane (Caterpillar Inc.) for providing the spray specimens and Dennis Turczyn (Caterpillar Inc.) for the surface profile measurements.

References

1. C.Y. Jian, T. Hashida, H. Takahashi, and M. Saito: "Thermal Shock and Fatigue Resistance Evaluation of Functionally Graded Coating for Gas Turbine Blades by Laser Heating Method," *Compos. Eng.*, 1995, *5*(7), pp. 879-89.
2. H. Balke, I. Hofinger, C. Häusler, H.-A. Bahr, H.-J. Weiß, and G. Kirchhoff: "Fracture Mechanical Damage Modelling of Thermal Barrier Coatings," *Arch. Appl. Mech.*, 2000, *70*, pp. 193-200.
3. I. Hofinger, M. Oechsner, H.-A. Bahr, and M.V. Swain: "Modified Four-Point Bending Specimen for Determining the Interface Fracture Energy for Thin, Brittle Layers," *Int. J. Fract.*, 1998, *92*, pp. 213-20.
4. I. Hofinger, H.-A. Bahr, H. Balke, G. Kirchhoff, C. Häusler, and H.-J. Weiß: "Fracture Mechanical Modelling and Damage Characterization of Functionally Graded Thermal Barrier Coatings by Means of Laser Irradiation," *Mater. Sci. Forum*, 1999, *308-311*, pp. 450-56.
5. M. Hollatz, M. Bobeth, and W. Pompe: "Failure of Alumina Scales on NiAl Under Graded Scale Loading," *Mater. Corros.*, 1996, *47*, pp. 633-45.
6. R.C. Brink: "Material Property Evaluation of Thick Thermal Barrier Coating Systems," *J. Eng. Gas Turbines Power*, 1989, *111*(7), pp. 570-77.
7. C.C. Berndt: "Thermally Sprayed Coatings: Properties and Applications" in *Surface Modification Technologies IV*, T.S. Sudarshan, D.G. Bhat, and M. Jeandin, ed., The Materials and Metals Society, Warrendale, PA, 1991, pp. 193-213.
8. K.F. Wesling, D.F. Socie, and M.B. Beardsley: "Fatigue of Thick Thermal Barrier Coatings," *J. Am. Ceram. Soc.*, 1994, *77*(7), pp. 1863-68.
9. M.S. Hu and A.G. Evans: "The Cracking and Decohesion of Thin Films on Ductile Substrates," *Acta Metall.*, 1989, *37*(3), pp. 917-25.
10. P.G. Charalambides, J. Lund, A.G. Evans, and R.M. McMeeking: "A Test Specimen for Determining the Fracture Resistance of Bimaterial Interfaces," *J. Appl. Mech.*, 1989, *56*, pp. 77-82.
11. A. Cazzato and K.T. Faber: "Fracture Energy of Glass-Alumina Interfaces Via the Bimaterial Bend Test," *J. Am. Cer. Soc.*, 1997, *80*(1), pp. 181-88.
12. J.W. Hutchinson and Z. Sou: "Mixed Mode Cracking in Layered Materials," *Adv. Appl. Mech.*, 1992, *29*, p. 63.
13. A.G. Evans, M. Rühle, B.J. Dalgleish, and P.G. Charalambides: "The Fracture Energy of Bimaterial Interfaces," *Mater. Sci. Eng.*, 1990, *A126*, pp. 53-64.